Four-dimensional ultrasound current source density imaging of a dipole field

Z. H. Wang,[1] R. Olafsson,[2] P. Ingram,[1] Q. Li,[1] Y. Qin,[1] and R. S. Witte[1,a)]
[1]*Department of Radiology, University of Arizona, Tucson, Arizona 85724, USA*
[2]*Electrical Engineering, University of Iceland, Reykjavik 107, Iceland*

(Received 12 April 2011; accepted 2 August 2011; published online 14 September 2011)

Ultrasound current source density imaging (UCSDI) potentially transforms conventional electrical mapping of excitable organs, such as the brain and heart. For this study, we demonstrate volume imaging of a time-varying current field by scanning a focused ultrasound beam and detecting the acoustoelectric (AE) interaction signal. A pair of electrodes produced an alternating current distribution in a special imaging chamber filled with a 0.9% NaCl solution. A pulsed 1 MHz ultrasound beam was scanned near the source and sink, while the AE signal was detected on remote recording electrodes, resulting in time-lapsed volume movies of the alternating current distribution. © *2011 American Institute of Physics*. [doi:10.1063/1.3632034]

Electrical mapping helps identify abnormal electric pathways in the heart (i.e., arrhythmias) and brain (i.e., epileptic seizures) during treatment.[1,2] This invasive procedure requires assumptions for reconstructing the current distribution, has limited spatial resolution, and is sensitive to registration errors.[3] Ultrasound current source density imaging (UCSDI) has been proposed as a complement and possible alternative to traditional mapping of electrophysiological signals.[4–11] UCSDI exploits the acoustoelectric effect (AE), an interaction between pressure and current, to map electric field distributions while scanning a focused ultrasound beam. A previous study in the rabbit heart demonstrated that UCSDI has sufficient sensitivity to map the cardiac activation wave.[4] Potential advantages of UCSDI include 1) remote detection of current with a spatial resolution determined by the size of the ultrasound focus (<5 mm^3); 2) volume images of current flow and biopotentials with as few as one electrode and ground without major assumptions regarding conductivity; 3) automatic coregistration of UCSDI with pulse echo (PE) ultrasound for simultaneously portraying current flow with anatomy. This study demonstrates volume imaging of a time-varying current field produced by scanning an ultrasound beam and detecting the generated AE signal.

UCSDI is based on reciprocal theory.[4,6,11] In an electric field produced from a distributed current source $\mathbf{J}^I = \mathbf{J}^I(x, y, z; t_s)$ changing in physiologic time t_s, the voltage V_i measured by lead i at coordinate x_0, y_0, z_0 can be expressed in four dimensions under the assumption of far field detection of the AE signal. If an ultrasound beam is centered at $C(x_0, y_0, z_0)$, then any point (x, y, z) in the pressure field can be represented in the electric field as $(x+x_0,\ y+y_0,\ z+z_0)$. The induced AE voltage (V^{AE}) detected by two distant electrodes can be represented by

$$V_i^{AE}(x_0, y_0, t; t_s) = -P_0 \int\int\int K_I \rho_0 (\mathbf{J}_i^L \bullet \mathbf{J}^I)(x + x_0, y + y_0, z + z_0; t_s) \left[b(x, y, z) a\left(t - \frac{z}{c}\right) \right] dx dy dz, \quad (1)$$

with pressure pulse amplitude P_0, interaction constant K_I, resistivity ρ_0, current distribution of detector $\mathbf{J}_i^L(x, y, z)$, ultrasound beam pattern $b(x, y, z)$ defined with the transducer at the origin, speed of sound c, ultrasound pulse waveform $a(t\text{-}z/c)$, and fast ultrasound time t. The instantaneous local field potential is reconstructed by demodulating (or basebanding) the AE signal.

The current density J^I of the dipole is modeled as the gradient of the AE voltage.

$$J^I(x, y, z; t_s) \approx -\sigma_i \nabla V_i(x, y, z; t_s), \quad (2)$$

where ∇ is the gradient operator and σ_i is the local conductivity. The current source is the divergence of current density or Laplacian of the AE voltage

$$I_{CSD}(x, y, z; t_s) = -\nabla \bullet J^I(x, y, z; t_s) \approx \sigma_i \Delta V_i(x, y, z; t_s). \quad (3)$$

A multi-electrode chamber was designed in Solidworks® and fabricated on a three-dimensional (3-D) printer (Objet, Connex 350) for controlled experiments in saline (Figs. 1(a) and 1(b)). Stimulating and recording electrodes could be placed anywhere on an XY grid (5 mm spacing) and individually adjusted along Z.[10] Figure 1(c) depicts the instrumentation for generating the dipole and capturing the AE and PE signals. A waveform generator (HP33120) and pair of platinum electrodes produced a 3-cycle burst at 200 Hz, a rate similar to a fast depolarizing event in the heart or brain. A pulse/receiver (Panametrics 5077) excited a single-element focused transducer (1 MHz, d = 38 mm, f = 68 mm) with a peak negative pressure of 500 kPa at a repetition rate of 2500 Hz. The pressure full-width-half maximum (FWHM) of the focal zone was 2.8 mm (axial) and 3.9 mm (lateral), as measured with a commercial hydrophone (Onda Corp., HDL-200). The AE signal was detected on the Ag/AgCl recording electrodes, which were arranged near the dipole while the ultrasound transducer was scanned in the XY plane (Δx, $\Delta y = 0.5$ mm). The anode was used as a ground reference. At each position, a burst of 50 ultrasound pulses ($\Delta t_s = 400\ \mu s$) was produced, starting 2 ms before the onset of the injected current waveform and ending 20 ms later. For each ultrasound trigger, the PE signal was also acquired by the ultrasound transducer. The multichannel data acquisition system (NI PXI- 5105) recorded the AE and PE signals (Fig. 1(c)). The injected current waveform was recorded by measuring the

a)Electronic mail: rwitte@email.arizona.edu.

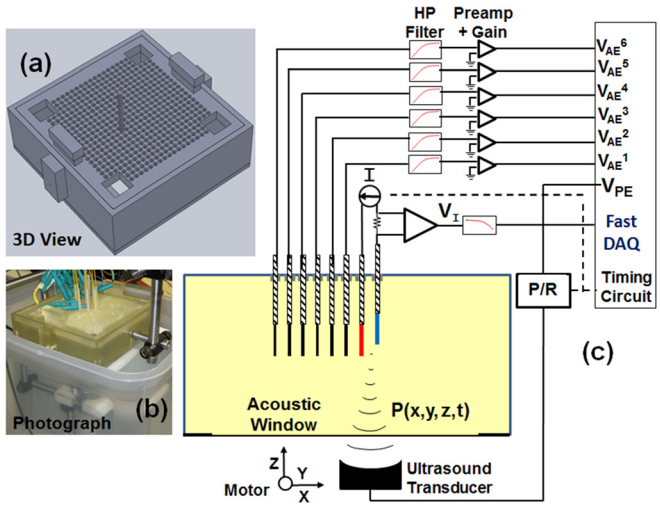

FIG. 1. (Color online) Apparatus for 4-D Multichannel UCSDI. (a) Custom multielectrode chamber designed in SolidWorks®. (b) Photograph of chamber fabricated on a 3D printer with electrodes in position and ultrasound transducer underneath. (c) Instrumentation for multichannel detection of the AE signal, low frequency current, and pulse echo signal. The ultrasound probe was scanned in an XY plane to produce volume datasets of the current field, as well as PE ultrasound images depicting the tips of the electrodes [P/R = pulser/receiver, DAQ = digital acquisition].

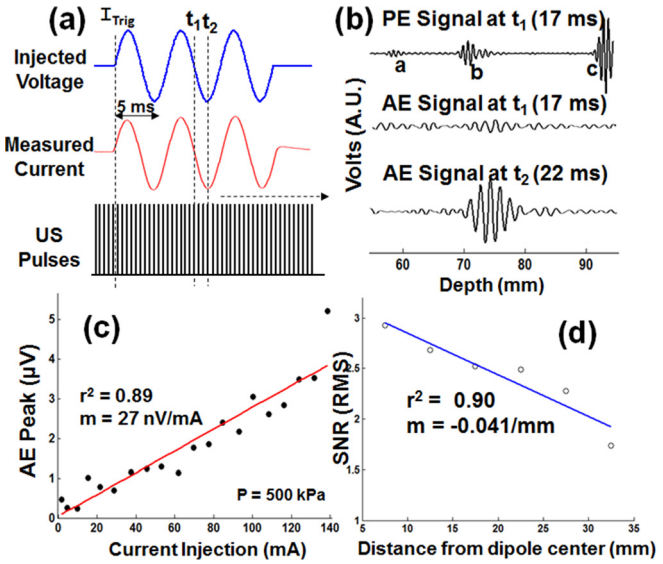

FIG. 2. (Color online) (a) Timing diagram for bursting ultrasound pulses during the injected current waveform. (b) Sample A lines at times denoted by dashed vertical lines in (a). The PE signal reveals the acoustic window [a], electrode [b], and saline/air boundary [c]. The AE and PE signals were sampled at 15 MHz and converted to distance based on the speed of sound and one way (AE) or two way (PE) travel of the same ultrasound pulse. (c) AE signal amplitude recorded on E_1 vs. amplitude of the current injection. (d) Effect of distance between recording electrode and center of dipole on SNR averaged across all current levels.

voltage across a 1 Ω resistor and digitized on an acquisition board (NI PXI 6289). The current dipole field was modeled using COMSOL™ and Matlab™ for direct comparison with the UCSDI experiments. Simulations considered the dielectric properties of saline and geometry of the electrodes, which are consistent with the experiments (cylinders with radius 0.15 mm and length 3 mm).

The timing sequence for UCSDI and sample A lines at one position of the ultrasound beam are presented in Figs. 2(a) and 2(b). While the PE signal relates to physical boundaries, the AE signal is proportional to the phase and amplitude of the local current density (Fig. 2(c)), consistent with theory and previous studies.[4–10] Also, a gradual decrease in the AE signal was observed on distant recording electrodes (Fig. 2(d)) relative to the ground reference. Signal to noise ratio (SNR) might be improved by averaging across several recording electrodes or applying higher pressure up to the limits of safe ultrasound exposure for imaging.

Fig. 3 exhibits Color M mode UCSDI at one position near the dipole ($i = 140$ mA). Each vertical line represents the sign and envelope of the instantaneous current density produced by demodulating and basebanding the AE signal. Whereas each vertical line denotes local current density along Z at a particular time, each horizontal line denotes the time waveform of the injected current at each depth position. Bandpass filters were applied along fast (1 MHz) and slow (200 Hz) time.

Figure 4 presents Color B mode UCSDI (Fig. 4(a)) of the current distribution at two different dipole orientations (0° and 44.2°), along with 3-D current projections and Laplacian (Fig. 4(b)). Eight recording electrodes were arranged in a circle with the dipole at the center. These two-dimensional images clearly illustrate the amplitude, orientation, and sign of the dipole. The dimensions (FWHM) of the reconstructed current dipole were 3.9 mm (lateral) and 4.9 mm (depth). Figure 5 depicts the top XY view of the reconstructed dipole (Fig. 5(a)) determined by scanning the ultrasound beam along the lateral plane. This figure also includes the co-registered PE ultrasound image (Fig. 5(b)), revealing the location of all electrodes, and superimposed image (Fig. 5(c)). Although eight recording electrodes are depicted, only one electrode (E_1) and a ground were used to produce the UCSDI representation of the time-varying dipoles at two different orientations. Complete four-dimensional (4-D) UCSDI multimedia movies are available online (Figs 5(a)–5(c)).

Figure 6 compares the measured UCSDI (Fig. 6(a)) and Laplacian images (Figs. 6(b) and 6(c)) of the current source with the simulated images at the time of peak current. The voltage potential in the simulation was determined from the inner product of the electric field between the dipole and detector E_1. The measured and modeled low frequency voltage

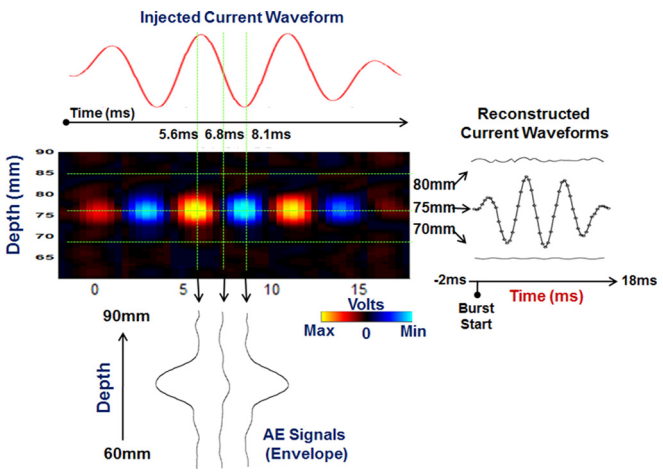

FIG. 3. (Color online) Color M Mode UCSDI: time varying image of demodulated AE voltage during current burst. (Right) Time varying waveforms at different depths. (Bottom) Envelope and sign related to the local current density at three time points.

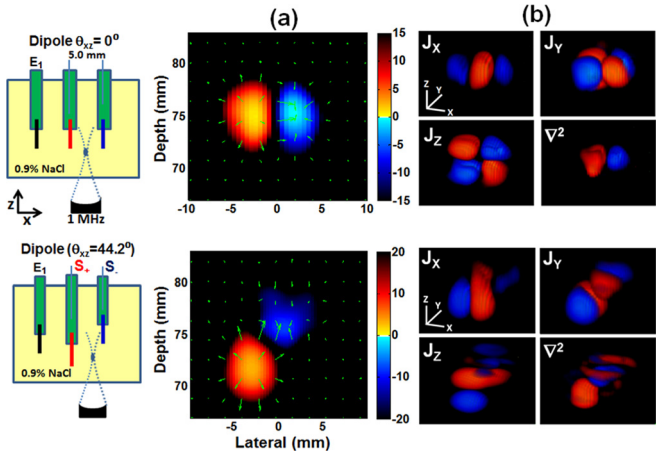

FIG. 4. (Color online) (a) Color B Mode UCSDI recorded on a single electrode for two dipole orientations at $t_s = 11$ ms, along with (b) J current projections J^I_x, J^I_y, and J^I_z and Laplacian. The image is displayed on a hot-cold color map with a dynamic range of ±20 dB.

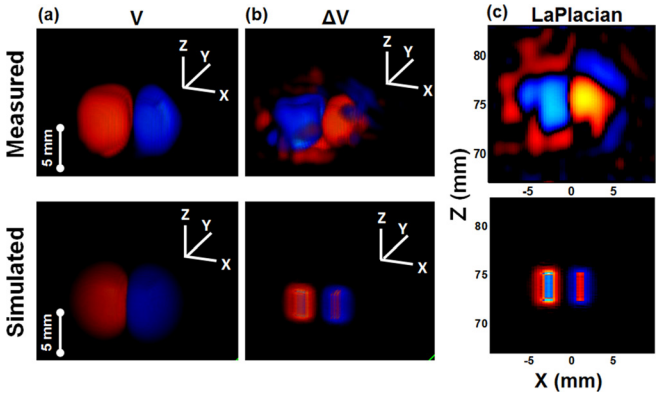

FIG. 6. (Color online) Comparison between measured (UCSDI) and modeled (COMSOL) images of the current dipole in saline. (a) Voltage potential; (b) Current source from Laplacian of (a); (c) XZ plane through center of Laplacian image. Source and sink represent the cathode and anode position of the original dipole. Electrode tips were at Z = 75 mm. A wide dynamic range is displayed to help visualize the complete field distribution pattern.

images (left column) appear almost identical. However, the Laplacian of the measured UCSDI is considerably larger than the actual current source and sink represented by the platinum electrodes. This can be explained by the filtering effect of the ultrasound beam and the dependence of the ultrasound focus on the spatial resolution of UCSDI.[6] The lateral and axial dimensions of the measured Laplacian image of 3.1 × 3.2 mm (FWHM) were close to the dimensions of the ultrasound focus (2.8 × 3.9 mm).

This study demonstrated that a focused ultrasound beam combined with a single recording electrode and ground reference is sufficient to produce volume images of a time-varying current distribution in conductive media. This complements earlier studies reporting that UCSDI has sufficient sensitivity to detect biologically relevant current in cardiac and neural tissue at safe levels of acoustic exposure for imaging.[4,5] The mechanical index (MI) is typically employed to quantify acoustic exposure for short ultrasound pulses at a low duty cycle. MI is defined as $P_{neg}/\sqrt{f_c}$, where P_{neg} is peak negative pressure and f_c is center frequency in MHz. The images in this report were acquired using an MI of 0.5, less than the maximum safe exposure of 1.9 for diagnostic imaging.[12] Most ultrasound probes designed for cardiac echocardiography are capable of delivering comparable ultrasound pressure directly to the heart.

One limitation with this study was the slow scan time (>1 h) necessary to obtain a 4D dataset. The primary bottleneck was due to mechanical translation of the motors along the XY plane. However, real-time UCSDI is potentially possible with a probe array and electronic beam steering—a common feature on most clinical ultrasound systems. Modern scanners employ fast frame rates for B mode imaging (>300 Hz) and those featuring a planar probe acquire 3-D images near 50 Hz. Similar frames rates are theoretically possible for UCSDI, because it can be performed simultaneously with PE imaging. A fast dual modality system capable of both UCSDI and echocardiography would be a powerful tool for tracking mechanical and electrical cardiac events. UCSDI also potentially simplifies electrical brain imaging by identifying the source of seizures and critical brain regions during the treatment of epilepsy.

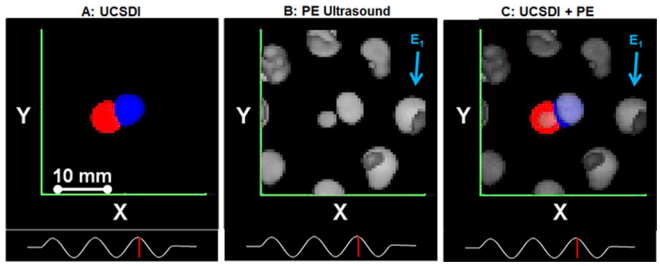

FIG. 5. (Color online) (a) A single UCSDI frame (top XY view) using the detector located at E_1 at $t_s = 11$ ms. (b) Corresponding PE ultrasound image denoting location of all electrodes. (c) Superimposed UCSDI and PE image from (a) and (b). Bottom: current injection time waveform (3 cycle burst at 200 Hz). Median (n = [3,3]) and Gaussian smoothing filters ($\sigma = 1$ mm) were applied along X and Y to improve SNR (enhanced online) [URL: http://dx.doi.org/10.1063/1.3632034.1; http://dx.doi.org/10.1063/1.3632034.2; http://dx.doi.org/10.1063/1.3632034.3].

We appreciate funding support from NIH (R01EB009353), Technology and Research Initiative Fund and Advanced Research Institute for Biomedical Imaging.

[1]F. Morady, J. Cardiovasc. Electrophys. **15**(1), 124 (2004).
[2]J. Engel, J. Epilepsy Curr. **3**, 37 (2003).
[3]H. Klemm, Ind. Pacing Electrophys. J. **7**(3), 148 (2007).
[4]R. Olafsson, R. S. Witte, C. Jia, S.-W. Huang, K. Kim, and M. O'Donnell, IEEE Trans. Ultrason. Ferroelectr. Freq. Control **56**(3), 565–574 (2009).
[5]R. S. Witte, R. Olafsson, and M. O'Donnell, Appl. Phys. Lett. **9**(90), 163902 (2007).
[6]R. Olafsson, R. S. Witte, S. W. Huang, and M. O'Donnell, IEEE Trans. Biomed. Eng. **55**(7), 1840–1848 (2008).
[7]R. Olafsson, Q. Li, Z. H. Wang, P. Ingram, and R. S. Witte, IEEE Ultrasonics Symposium, 20–23 September 2009, pp. 333–336.
[8]R. S. Witte, T. Hall, S.-W. Huang, R. Olafsson, and M. O'Donnell, J. Appl. Phys. **104**, 054701 (2008).
[9]Z. H. Wang, P. Ingram, R. Olafsson, Q. Li, and R. S. Witte, Proc. SPIE **7629**, 76290H (2010).
[10]Z. H. Wang, R. Olafsson, P. Ingram, Q. Li, and R. S. Witte, IEEE Ultrasonics Symposium, 11–14 October 2009, pp. 253–256.
[11]R. Yang, X. Li, J. Liu, and B. He, Phys. Med. Biol. **56**(13), 3825 (2011).
[12]Food and Drug Administration, *Information for Manufacturers Seeking Marketing Clearance of Diagnostic US systems and Transducers*, Rockville, MD, Sept. 8, 2008 (1997).